Transverse optic modes in monoclinic α-Bi_2O_3

1996 J. Phys.: Condens. Matter 8 6199

(http://iopscience.iop.org/0953-8984/8/34/010)

J. Phys.: Condens. Matter **8** (1996) 6199–6212. Printed in the UK

Transverse optic modes in monoclinic α-Bi_2O_3

A B Kuz'menko†, E A Tishchenko† and V G Orlov‡

† P L Kapitza Institute for Physical Problems, Russian Academy of Science, 117334 Moscow, Russia

‡ Russian Kurchatov Institute Research Centre, 123182, Moscow, Russia

Received 7 May 1996

Abstract. Measurements of infrared polarized reflectance spectra of single-crystal α-Bi_2O_3 have been made at room temperature in the wavelength range from 30 to 4000 cm^{-1} for different orientations of the wave vector $\boldsymbol{k}$ and the electric field $\boldsymbol{E}$ of the incident radiation relative to the crystallographic axes. On the basis of Born and Huang's theory, relations between characteristics of TO modes of the monoclinic lattice and the reflectivity for the orientations used are established. Dipole momentum orientations, frequencies, strengths and linewidths of almost all of the IR-active modes predicted by the factor-group analysis for the α-Bi_2O_3 were determined. Good agreement between experimentally measured and model spectra was achieved. It was shown that in order to obtain reliable values of parameters of B_u modes three spectra for different orientations of $\boldsymbol{E}$ in the ac-plane should be fitted simultaneously. It was found that B_u modes have significantly greater intensities than A_u modes. The effect of the rotation of the principal dielectric axes within the ac-plane was studied.

1. Introduction

A study of the bismuth oxide vibrational spectra is of special interest nowadays because this compound is a parent substance for several families of high-T_c superconductors: the copper-containing layered compounds Bi–Sr–Ca–Cu–O [1, 2] and copper-free perovskite-type substances $BaPb_{1-x}Bi_xO_3$ [3] and $Ba_{1-x}K_xBiO_3$ [4, 5]. Several groups have presented infrared as well as Raman spectra of Bi_2O_3 [6, 7, 8, 9]. All of the spectra were measured only for polycrystalline samples. In [6, 9] the IR absorption spectra were measured and in [7] the IR reflectance spectrum was reported. The existence of a large number of IR-active lines in a limited energy range embarrassed determination of their characteristics. In the polycrystalline spectrum, modes of all species are presented simultaneously; therefore it was practically impossible to make an assignment of each particular line. For this reason we used a single-crystal sample of α-Bi_2O_3 and studied reflectance spectra for different orientations of the wave vector $\boldsymbol{k}$ and the electric field $\boldsymbol{E}$ of the incident wave relative to the crystallographic axes in order to obtain full information about lattice vibrations. Our polarized spectra revealed large anisotropy of dielectric properties of α-Bi_2O_3 in accordance with the complicated structure of its primitive cell.

The α-phase of the bismuth oxide has the monoclinic structure (space group $P2_1/c$, or C_{2h}^5) [10]. A unit cell of α-Bi_2O_3 contains four formula units; each atom is arranged in a position of general type. Factor-group analysis enables one to classify the optical vibrational spectrum of α-Bi_2O_3 in the following way [10]: 30 modes ($15A_g + 15B_g$) are active in the Raman scattering; 27 optical vibrations ($14A_u + 13B_u$) manifest themselves in the infrared spectra. Selection rules for the IR-active vibrations [11] lead to the conclusion that dipole

0953-8984/96/346199+14$19.50

momenta of the A_u modes are oriented along the ***b***-axis and the B_u modes have momenta lying in the *ac*-plane. Due to the presence of the inversion centre, IR and Raman modes are mutually exclusive.

The compound α-Bi_2O_3 belongs to the class of optically biaxial crystals. The principal values of its dielectric tensor $\hat{\epsilon}(\omega)$ are all different. In the monoclinic crystal one of the principal dielectric axes coincides with the ***b***-axis; the others lie in the *ac*-plane, but their directions are not determined by the symmetry considerations. Moreover, it turns out that the directions of these axes depend on frequency [11]. Therefore, conventional dispersion analysis [12, 13], based on the scalar relations between the electric field $\boldsymbol{E}$ and polarization $\boldsymbol{P}$, can be applied for determination of the characteristics of A_u modes only. Correct values of B_u-mode parameters can be obtained by analysis of several reflectance spectra for the vector $\boldsymbol{E}$ lying in the *ac*-plane, using formulas for the dielectric tensor and reflectivity which take into account rotation of principal axes. We have introduced for B_u modes, along with the usual frequency, strength and linewidth, an additional angle parameter describing the direction of the dipole momentum associated with a particular lattice vibration. The reflectivity for the geometries used was expressed on the basis of these parameters using Born and Huang's theory of crystal dynamics [14] and principles of crystal optics [15, 16]. The simulation of all of the measured spectra by adjustment of the above-mentioned phonon parameters was performed on the basis of established relations. We succeeded in obtaining good quantitative agreement between the model and experimental spectra by introducing a reasonable number of modes, which confirms the validity of the proposed model. In this paper we shall describe this model in detail, and focus on the peculiarities of the corresponding technique of mode characteristic determination. Then we will discuss the parameters obtained for the TO modes of α-Bi_2O_3. At the end we will analyse to what extent the effect of dielectric axis rotation is exhibited in the far infrared.

2. Experimental details

Single-crystal α-Bi_2O_3 was obtained by hydrothermal synthesis in alkaline water solutions. Synthesis was carried out in an autoclave at a temperature of about 573 K and pressure of 8 MPa. The x-ray spectral microanalysis performed with the spectrometer CAMEBAX-301 demonstrated the absence of impurities in the crystal with an accuracy of about 0.01 wt%. At room temperature the unit-cell parameters of the monoclinic crystal lattice $a = 5.8504$ Å, $b = 8.1708$ Å, $c = 7.5136$ Å, $\beta = 113^\circ$ were in agreement with the previously published data [10]. The crystal had a good-quality natural face nearly parallel to the *ac*-plane (with an accuracy of $\sim 4^\circ$) having dimensions of about 4×7 mm. An additional side parallel to the ***b***-axis and perpendicular to the ***a***-axis with the dimensions 1.5×7 mm was cut and mechanically polished.

The reflectance spectra were studied using two grating-type spectrophotometers, IR-460 (4000–400 cm^{-1}) and FIS-3 (400–30 cm^{-1}), each having a special reflection attachment constructed after the monochromator. A set of light sources, detectors and grid polarizers with overlapping working ranges were used. The polarizer was mounted between the monochromator and the sample. The varying of the polarization angle was performed by rotation of the polarizer; the orientation of the sample was always fixed relative to the optical set-up. The infrared beam was focused on the crystal surface at an average incidence angle of about 15°. A special manipulator was designed to automatically interchange the sample and a gold mirror with good accuracy. In the far-infrared region, when measurements were executed slowly with large accumulation, the sample and mirror were interchanged at any frequency point to remove the influence of the signal drift. The spectral slit width was

maintained to be within about 1–2% of the wavelength. The noise-to-signal ratio varied from 1 to 4% (in several spectral regions the signal was noticeably diminished as a result of the double attenuation of the light by the monochromator and the polarizer). The degree of polarization was better than 95% for all wavelengths.

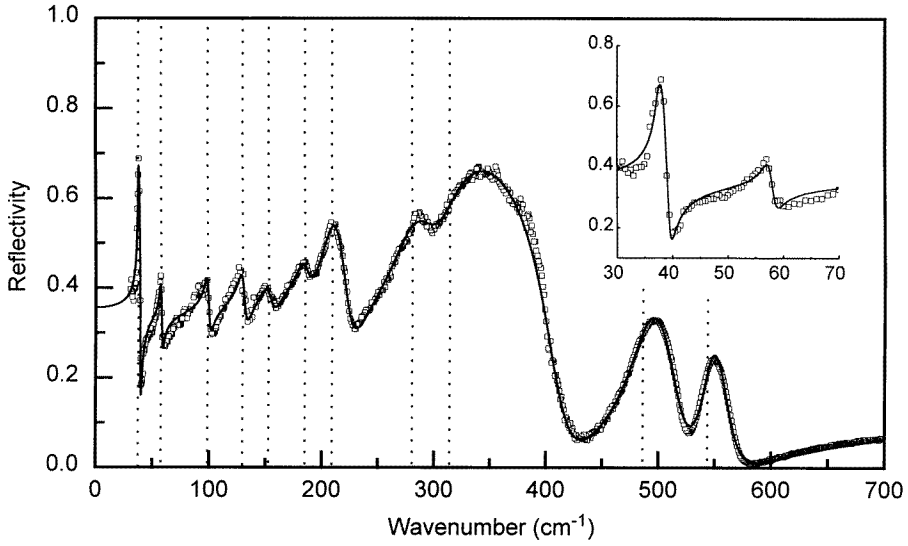

Figure 1. The reflectance spectrum, measured at room temperature when the electric field $\boldsymbol{E}$ of the incident radiation was directed along the $\boldsymbol{b}$-axis. Experimental points are shown by open squares. The solid curve corresponds to the model spectrum for parameters of A_u modes, presented in table 1. Vertical lines mark the frequencies of modes that were obtained. In the inset the low-frequency part of the spectrum is shown.

In figures 1 and 2 four reflectance spectra measured at room temperature in different reflecting geometries are presented for the range 30–700 cm^{-1}, where all the phonon frequencies are observed. In the first case (figure 1) light was reflected from the face oriented perpendicular to the $\boldsymbol{a}$-axis. The electric field $\boldsymbol{E}$ of the incident radiation was directed along the $\boldsymbol{b}$-axis. The other three spectra (figures 2(a)–2(c)) were measured when the reflection was from the $\boldsymbol{a}$–$\boldsymbol{c}$-face. The angle χ between the direction of $\boldsymbol{E}$ and the $\boldsymbol{a}$-axis was 0°, 45° and 90° respectively (all of the angles introduced in the current paper, which describe the orientation of a certain vector within the ac-plane, were measured anticlockwise relative to the $\boldsymbol{a}$-axis; see figure 3). The particular choice of reflectance geometries was determined by considerations discussed in section 4. We can see from figure 2 that the varying of the electric field direction within the ac-plane results in a very strong variation of the spectrum shape. For example, the value of reflectivity at 310 cm^{-1} varies from 0.15 for $\chi = 0°$ to 0.8 for $\chi = 90°$. Before discussion of the experimental data and their numerical analysis we shall introduce a simple model which links reflectivity with phonon parameters of the monoclinic lattice.

3. The dielectric tensor in the far infrared

Born and Huang in their fundamental work [14] have given a phenomenological and microscopic description of the lattice dynamics in the infrared region. They have shown that

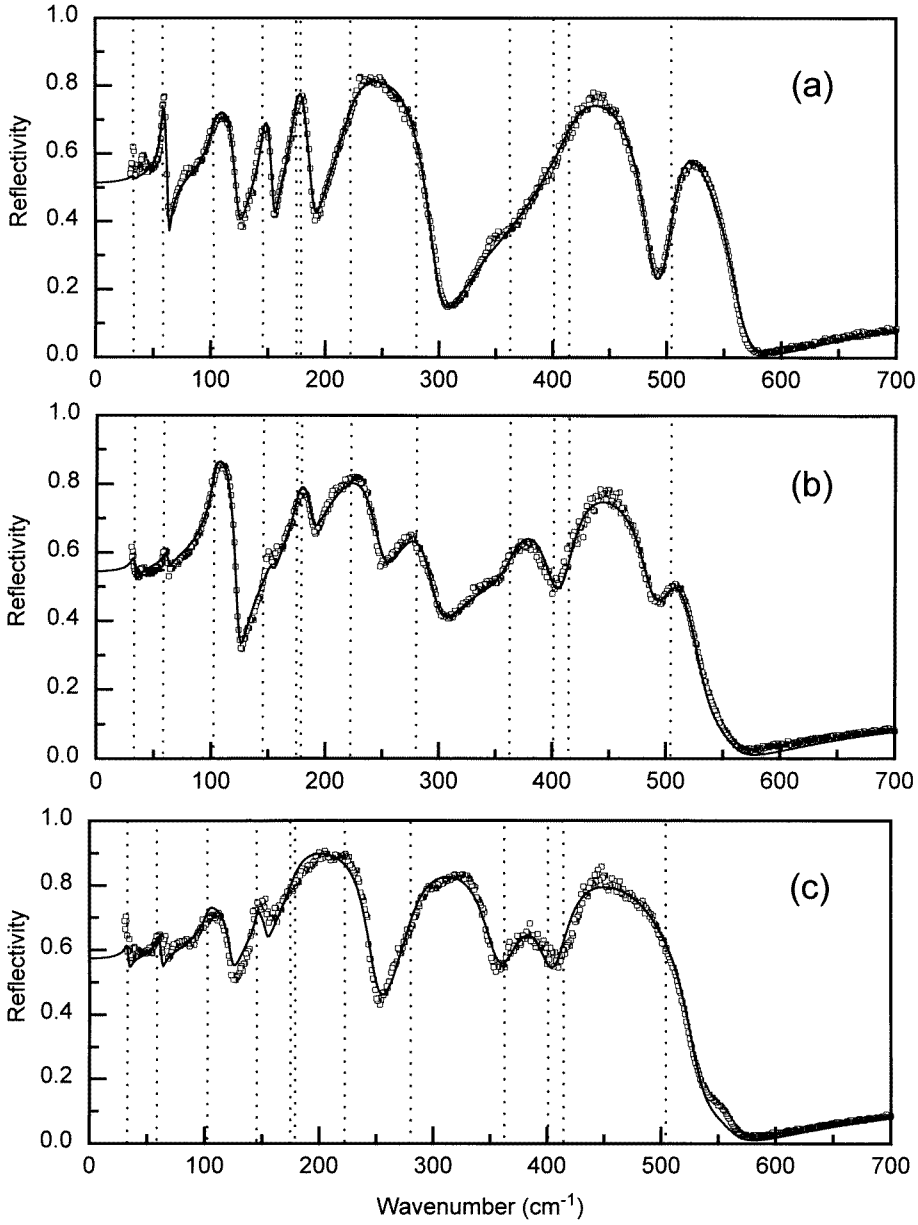

Figure 2. Reflectance spectra, measured at room temperature for different directions of the electric field $\boldsymbol{E}$ of the incident radiation within the ac-plane. The direction is described by the angle χ between the vector $\boldsymbol{E}$ and the $\boldsymbol{a}$-axis. (a) $\chi = 0^\circ$; (b) $\chi = 45^\circ$; (c) $\chi = 90^\circ$. Experimental points are shown by open squares. Solid curves correspond to the model spectra for parameters of B_u modes, presented in table 1. Vertical lines mark the frequencies of modes that were obtained.

both approaches lead to the following tensor of the dielectric function $\hat{\epsilon}(\omega)$ ($\alpha, \beta = x, y, z$):

$$\epsilon_{\alpha\beta}(\omega) = \epsilon_{\alpha\beta}^{\infty} + 4\pi \sum_j \frac{M_{j\alpha} M_{j\beta}}{\omega_{0j}^2 - \omega^2 - \mathrm{i}\gamma_j \omega} \tag{1}$$

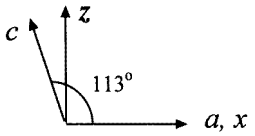

Figure 3. The relative arrangement of the cartesian ($\boldsymbol{x}, \boldsymbol{y}, \boldsymbol{z}$) and crystallographic ($\boldsymbol{a}, \boldsymbol{b}, \boldsymbol{c}$) systems of coordinates. The axes $\boldsymbol{y}$ and $\boldsymbol{b}$ are collinear and directed away from the reader.

where ω_{0j}, γ_j, and $\boldsymbol{M}_j$ are the frequency, damping coefficient, and effective dipole momentum corresponding to the j-mode (the summation is performed over all of the IR-active modes); $\epsilon^{\infty}_{\alpha\beta}$ is the contribution from the high-frequency electronic excitations. Rigorous microscopic analysis of the dissipation caused by the potential anharmonicity gives frequency-dependent γ_j [14, 17]. However, an approximation in which γ_j is supposed to be constant is widely used. Justification of such an approach may be found, e.g., in [13]. In this paper we shall also set γ_j as a constant mode parameter. So we shall not directly consider multi-phonon resonances, which should be described by a theory of the next order.

It is important that due to the existence of the macroscopic electric field caused by the longitudinal component of the lattice polarization, all phonon parameters depend on the direction of the wave vector $\boldsymbol{k}$ even when $|\boldsymbol{k}| \to 0$ [14]. One can eliminate this ambiguity by consideration of only TO vibrations. Orientations of the crystal surface and the incident radiation were always chosen so that the vectors of the electric field $\boldsymbol{E}$, displacement $\boldsymbol{D}$ and polarization $\boldsymbol{P}$ were perpendicular to the wave vector $\boldsymbol{k}$. In this case the electromagnetic wave interacts only with TO lattice modes.

According to expression (1), the contribution of each vibrational mode to the infrared properties of the anisotropic crystal is in general described by five real parameters: ω_j, γ_j and three components of $\boldsymbol{M}_j$. Using symmetry considerations it is possible to reduce this number; that is, vector $\boldsymbol{M}_j$ for each A_u mode has only one component parallel to the $\boldsymbol{b}$-axis; the direction of the B_u-mode dipole momentum lying in the ac-plane can be described by one angle parameter.

Let us introduce now a cartesian right-handed system of coordinates xyz related to the crystallographic system as follows: $\boldsymbol{x} \parallel \boldsymbol{a}, \boldsymbol{y} \parallel \boldsymbol{b}, \boldsymbol{z} \perp \boldsymbol{x}$ and $\perp \boldsymbol{y}$ (figure 3). In this system the tensor $\hat{\epsilon}(\omega)$ has the following structure:

$$\hat{\epsilon} = \begin{pmatrix} \epsilon_{xx} & 0 & \epsilon_{xz} \\ 0 & \epsilon_{yy} & 0 \\ \epsilon_{zx} & 0 & \epsilon_{zz} \end{pmatrix}. \tag{2}$$

According to (1) non-zero components of (2) can be written in the form

$$\epsilon_{yy} = \epsilon^{\infty}_{yy} + \sum_{A_u \text{ modes}} \frac{\omega^2_{pj}}{\omega^2_{0j} - \omega^2 - i\gamma_j\omega} \tag{3}$$

$$\epsilon_{xx} = \epsilon^{\infty}_{xx} + \sum_{B_u \text{ modes}} \frac{\omega^2_{pj} \cos^2\theta_j}{\omega^2_{0j} - \omega^2 - i\gamma_j\omega} \tag{4}$$

$$\epsilon_{zz} = \epsilon^{\infty}_{zz} + \sum_{B_u \text{ modes}} \frac{\omega^2_{pj} \sin^2\theta_j}{\omega^2_{0j} - \omega^2 - i\gamma_j\omega} \tag{5}$$

$$\epsilon_{xz} = \epsilon_{zx} = \epsilon^{\infty}_{xz} + \sum_{B_u \text{ modes}} \frac{\omega^2_{pj} \cos\theta_j \sin\theta_j}{\omega^2_{0j} - \omega^2 - i\gamma_j\omega}. \tag{6}$$

Here we have substituted for the effective dipole momentum with the corresponding plasma frequency $\omega^2_{pj} = 4\pi M^2_j$ and have introduced for each B_u mode the angle θ_j between vector

$\boldsymbol{M}_j$ and the x-axis.

4. Calculation of the reflectivity

Given model expressions for $\hat{\epsilon}(\omega)$, the reflectivity $R(\omega)$ for each geometry can be calculated using the boundary conditions $E_{1t} = E_{2t}$, $H_{1t} = H_{2t}$. In this section we shall always consider normal incidence of a linearly polarized plane wave onto the crystal surface. Different cases of reflectance geometry may be classified by the directions of the vectors $\boldsymbol{E}$ and $\boldsymbol{k}$ of the incident wave. The wave vector of the refracted wave is also perpendicular to the surface because the tangential component of $\boldsymbol{k}$ must be invariant. We shall analyse two special cases of reflectance geometry: $\boldsymbol{E} \parallel \boldsymbol{b}$, $\boldsymbol{k} \parallel (\boldsymbol{a}$–$\boldsymbol{c})$ and $\boldsymbol{E} \parallel (\boldsymbol{a}$–$\boldsymbol{c})$, $\boldsymbol{k} \parallel \boldsymbol{b}$. The reasons for this choice are: (i) the set of spectra under consideration must contain information about all of the vibrational modes; (ii) each spectrum should depend on only one mode species (A_u or B_u); (iii) the incident wave must excite only TO vibrations inside the crystal.

4.1. The case where $\boldsymbol{E} \parallel \boldsymbol{b}$, $\boldsymbol{k} \parallel (\boldsymbol{a}$–$\boldsymbol{c})$: probing of A_u modes

As the vector $\boldsymbol{E}$ is directed along the principal dielectric axis, the propagation of the electromagnetic wave inside the crystal occurs in the same manner as for the cubic crystal with $\epsilon = \epsilon_{yy}$. So, the direction of $\boldsymbol{k}$ within the ac-plane is of no importance. The reflectivity is given by the usual Fresnel formula for derived cubic crystals:

$$R = \left| \frac{\sqrt{\epsilon_{yy}} - 1}{\sqrt{\epsilon_{yy}} + 1} \right|^2$$

where ϵ_{yy} is determined by A_u modes only (equation (3)).

The conventional method of treatment of such a spectrum (dispersion analysis) is that of selecting the phonon parameters in (3) giving the best agreement between the model and the experimentally measured spectrum [12].

4.2. The case where $\boldsymbol{E} \parallel (\boldsymbol{a}$–$\boldsymbol{c})$, $\boldsymbol{k} \parallel \boldsymbol{b}$: probing of B_u modes

This case is more complicated than the first one, because the directions of the principal axes of $\hat{\epsilon}(\omega)$ in the ac-plane are not fixed. From Maxwell's equations and the boundary conditions an important conclusion follows: that the vectors $\boldsymbol{E}$, $\boldsymbol{D}$ and $\boldsymbol{P}$ of the refracted wave lie in the ac-plane. This means that only TO modes are excited.

It is well known [15, 16] that to a certain direction of $\boldsymbol{s} = \boldsymbol{k}/|\boldsymbol{k}|$ inside an anisotropic crystal there correspond exactly two waves with different refractive indices n and mutually perpendicular amplitudes of the electric field $\boldsymbol{E}$ (when this direction does not coincide with the optical axis). We shall designate all of the values corresponding to these waves by the subscripts u and v. The values n_u, n_v and vectors $\boldsymbol{E}_u$, $\boldsymbol{E}_v$ can be found by solving the algebraic system of equations [16, 17]

$$[\epsilon_{\alpha\beta} - n^2(\delta_{\alpha\beta} - s_\alpha s_\beta)]E_\beta = 0. \tag{7}$$

In our particular geometry, we shall consider only x- and z-components of the electric field because E_y is zero. In contrast, only s_y is non-zero. Hence the system (7) is simply the equation for the eigenvectors and eigenvalues of $\hat{\epsilon}$:

$$\begin{pmatrix} \epsilon_{xx} - n^2 & \epsilon_{xz} \\ \epsilon_{zx} & \epsilon_{zz} - n^2 \end{pmatrix} \begin{pmatrix} E_x \\ E_z \end{pmatrix} = 0.$$

Setting the determinant to zero, we obtain

$$n_{u,v}^2 = (1/2)(\epsilon_{xx} + \epsilon_{zz} \pm \sqrt{(\epsilon_{xx} - \epsilon_{zz})^2 + 4\epsilon_{xz}^2}).$$

As $\hat{\epsilon}$ is symmetrical, an orthogonality is operative: $(\boldsymbol{E}_u \cdot \boldsymbol{E}_v) = E_{ux}E_{vx} + E_{uz}E_{vz} = 0$. Let us consider normalized vectors $\boldsymbol{e}_{u,v} = \boldsymbol{E}_{u,v}/|\boldsymbol{E}_{u,v}|$. Their components can be written in terms of the angle φ between $\boldsymbol{E}_u$ and $\boldsymbol{x}$ (or between $\boldsymbol{E}_v$ and $\boldsymbol{z}$):

$$\boldsymbol{e}_u = \begin{pmatrix} \cos\varphi \\ \sin\varphi \end{pmatrix} \qquad \boldsymbol{e}_v = \begin{pmatrix} -\sin\varphi \\ \cos\varphi \end{pmatrix}.$$

Equation (7) is valid even for the case of strong relaxation (when the imaginary part is comparable with the real part of the dielectric function). As a result of damping, the x- and z-components of $\boldsymbol{E}_u$ and $\boldsymbol{E}_v$ are generally shifted in phase; this means that the corresponding waves are elliptically polarized. In this case the value of φ becomes complex. It is related to the components of $\hat{\epsilon}$ by a simple formula:

$$\tan 2\varphi = \frac{2\epsilon_{xz}}{\epsilon_{xx} - \epsilon_{zz}} = \left(2\epsilon_{xz}^{\infty} + \sum_j L_j \sin 2\theta_j\right) \Big/ \left(\epsilon_{xx}^{\infty} - \epsilon_{zz}^{\infty} + \sum_j L_j \cos 2\theta_j\right) \tag{8}$$

where we have denoted the Lorentzians $\omega_{pj}^2/(\omega_{0j}^2 - \omega^2 - \mathrm{i}\gamma_j\omega)$ for brevity by L_j.

Let us now present the electric field outside the crystal as a sum of incident and reflected waves (omitting the time factor $\exp(-\mathrm{i}\omega t)$):

$$\boldsymbol{E}_i \exp(\mathrm{i}\omega y/c) + \boldsymbol{E}_r \exp(-\mathrm{i}\omega y/c).$$

In the crystal volume, the waves $\boldsymbol{E}_u$ and $\boldsymbol{E}_v$ are excited:

$$E_u\boldsymbol{e}_u \exp(\mathrm{i}\omega n_u y/c) + E_v\boldsymbol{e}_v \exp(\mathrm{i}\omega n_v y/c).$$

To find E_u and E_v we need to consider the boundary conditions on the crystal surface (where we assume $y = 0$). They may be written in the form

$$\boldsymbol{E}_i + \boldsymbol{E}_r = E_u\boldsymbol{e}_u + E_v\boldsymbol{e}_v \tag{9}$$

$$\boldsymbol{E}_i - \boldsymbol{E}_r = n_uE_u\boldsymbol{e}_u + n_vE_v\boldsymbol{e}_v. \tag{10}$$

Using the orthogonality of $\boldsymbol{e}_u$ and $\boldsymbol{e}_v$, let us decompose the incident wave using them as a basis:

$$\boldsymbol{E}_i = (\boldsymbol{E}_i \cdot \boldsymbol{e}_u)\boldsymbol{e}_u + (\boldsymbol{E}_i \cdot \boldsymbol{e}_v)\boldsymbol{e}_v. \tag{11}$$

Substitution of (11) into the sum of (9) and (10) yields

$$E_{u,v} = \frac{2(\boldsymbol{E}_i \cdot \boldsymbol{e}_{u,v})}{1 + n_{u,v}}.$$

After subtraction of (10) from (9) we may immediately express $\boldsymbol{E}_r$ using $\boldsymbol{E}_i$:

$$\boldsymbol{E}_r = r_u(\boldsymbol{E}_i \cdot \boldsymbol{e}_u)\boldsymbol{e}_u + r_v(\boldsymbol{E}_i \cdot \boldsymbol{e}_v)\boldsymbol{e}_v \tag{12}$$

where the $r_{u,v} = (1 - n_{u,v})/(1 + n_{u,v})$ are complex reflectivities corresponding to the waves $\boldsymbol{E}_u$ and $\boldsymbol{E}_v$.

It is convenient to rewrite relation (12) in the form $\boldsymbol{E}_r = \hat{r}\boldsymbol{E}_i$, introducing the complex reflectivity matrix:

$$\hat{r} = \begin{pmatrix} r_ue_{ux}^2 + r_ve_{vx}^2 & r_ue_{ux}e_{uz} + r_ve_{vx}e_{vz} \\ r_ue_{ux}e_{uz} + r_ve_{vx}e_{vz} & r_ue_{uz}^2 + r_ve_{vz}^2 \end{pmatrix}$$

$$= \begin{pmatrix} r_u\cos^2\varphi + r_v\sin^2\varphi & (r_u - r_v)\cos\varphi\sin\varphi \\ (r_u - r_v)\cos\varphi\sin\varphi & r_u\sin^2\varphi + r_v\cos^2\varphi \end{pmatrix}. \tag{13}$$

The experimentally obtained reflectivity is the ratio between the intensities of the reflected and incident waves:

$$R = \frac{I_r}{I_i} = \frac{|E_{rx}|^2 + |E_{rz}|^2}{|E_{ix}|^2 + |E_{iz}|^2}. \tag{14}$$

To calculate the reflectivity it is necessary to introduce the angle χ between $\boldsymbol{E}_i$ and the x-axis:

$$\boldsymbol{E}_i = E_i \begin{pmatrix} \cos\chi \\ \sin\chi \end{pmatrix}. \tag{15}$$

Substituting in (15) and (14) using the matrix (13), after some transformations we can obtain the final expression for the reflectivity, containing φ and χ in the combination $\varphi - \chi$:

$$R = \left| \frac{r_u + r_v}{2} + \frac{r_u - r_v}{2} \cos 2(\varphi - \chi) \right|^2 + \left| \frac{r_u - r_v}{2} \sin 2(\varphi - \chi) \right|^2. \tag{16}$$

The following question arises: how many spectra for different angles χ should be measured to extract information about the parameters of B_u modes? Evidently, knowledge of only one spectrum is insufficient, because in comparison to the first case an excess of parameters is obtained. To remove this excess, measurement of several spectra must be performed. It turns out that when three spectra are known, measurement of an additional spectrum yields no extra information in the framework of the current model. To prove this, let us focus on the χ-dependence of the reflectivity. From (16) we may derive that $R(\chi)$ is an oscillating function with the period π:

$$R(\chi) = R_0 + A \sin 2\chi + B \cos 2\chi$$

where

$$R_0 = \left| \frac{r_u + r_v}{2} \right|^2 + \left| \frac{r_u - r_v}{2} \right|^2 (|\cos 2\varphi|^2 + |\sin 2\varphi|^2)$$

is the reflectivity of non-polarized light; we shall not write the cumbersome expressions for the coefficients A and B here. Suppose we have measured three spectra $R(\chi_1, \omega)$, $R(\chi_2, \omega)$, $R(\chi_3, \omega)$. As may be easily checked, the spectrum at any other angle χ can be presented as a linear composition:

$$R(\chi, \omega) = \alpha_1 R(\chi_1, \omega) + \alpha_2 R(\chi_2, \omega) + \alpha_3 R(\chi_3, \omega)$$

with ω-independent coefficients:

$$\alpha_1 = \frac{\sin(\chi - \chi_2)\sin(\chi - \chi_3)}{\sin(\chi_1 - \chi_2)\sin(\chi_1 - \chi_3)}$$
$$\alpha_2 = \frac{\sin(\chi - \chi_1)\sin(\chi - \chi_3)}{\sin(\chi_2 - \chi_1)\sin(\chi_2 - \chi_3)}$$
$$\alpha_3 = \frac{\sin(\chi - \chi_1)\sin(\chi - \chi_2)}{\sin(\chi_3 - \chi_1)\sin(\chi_3 - \chi_2)}.$$

In particular, the following relation holds:

$$R(0^\circ) + R(90^\circ) = R(45^\circ) + R(-45^\circ).$$

We have intentionally checked that within experimental errors this relation is satisfied for all wavelengths.

We have found that the most reliable values of phonon parameters can be obtained as a result of simultaneous fitting of three spectra for different angles of polarizations. In this work we have chosen the most natural set of angles: $\chi = 0^\circ$, 45° and 90°.

5. Results and discussion

The relations derived in the previous section were applied to the simulation of experimental spectra and the determination of the parameters of A_u and B_u modes of α-Bi_2O_3. In figures 1 and 2 model spectra are shown by solid curves. The fitting was carried out by the least-squares method. Minimization of χ^2 was performed by the Marquardt technique described in [18], with analytical calculation of the partial derivatives of χ^2 based on model parameters. Each experimental spectrum contained 1000 frequency points in the spectral region processed (30–1000 cm^{-1}). This was sufficient for introducing 11 A_u modes and 11 B_u modes to satisfactorily describe all essential spectral peculiarities; it is slightly less than the value that the factor-group analysis predicts: $14A_u + 13B_u$. The remaining three A_u modes and two B_u modes are possibly too weak to be observed; besides, some wide bands (especially ones with frequencies higher than 200 cm^{-1}) may be composed of several overlapping modes. For example, an additional weak mode with a frequency of about 400 cm^{-1} possibly should be added to the presented set of A_u modes, and a mode with a frequency of about 340 cm^{-1} possibly should be added to the set of B_u modes. The forthcoming experiments at low temperatures would probably make it possible to locate the missing modes.

Table 1. Characteristics of the observed IR-active TO modes obtained for α-Bi_2O_3.

Frequency ω_0 (cm^{-1})	Plasma frequency ω_p (cm^{-1})	Damping γ (cm^{-1})	Polarization angle θ	Strength ω_p^2/ω_0^2	Linewidth γ/ω_0
A_u modes					
37	47	1.1	—	1.59	0.030
58	34	2.0	—	0.35	0.034
99	61	3.9	—	0.38	0.039
130	88	6.0	—	0.45	0.046
153	99	11.5	—	0.41	0.075
185	140	12.3	—	0.57	0.066
209	299	17.8	—	2.04	0.085
280	463	36.5	—	2.72	0.130
314	453	44.8	—	2.08	0.142
486	302	32.6	—	0.38	0.067
544	161	18.6	—	0.09	0.034
B_u modes					
58	145	2.5	31°	6.10	0.042
102	422	6.8	−48°	17.0	0.067
145	417	3.8	48°	8.24	0.026
175	377	7.5	17°	4.64	0.043
179	847	17.3	−86°	22.4	0.097
222	616	22.7	12°	7.68	0.102
280	578	29.4	87°	4.26	0.105
362	377	33.9	−43°	1.08	0.094
401	622	30.8	23°	2.41	0.077
414	301	26.4	−39°	0.53	0.064
504	228	19.8	10°	0.20	0.039

Model parameters of the A_u and B_u modes are presented in table 1. Convenient dimensionless constants—the strength ω_p^2/ω_0^2 and relative linewidth γ/ω_0—are also presented for each mode. The mode frequencies obtained are shown in figures 1 and 2 by vertical dotted lines for comparison with the spectral peculiarities. The components of

the high-frequency dielectric tensor $\hat{\epsilon}^{\infty}$ were adjusted along with the other parameters. We found the following values for them: $\epsilon^{\infty}_{xx} = 6.2$, $\epsilon^{\infty}_{xz} = -0.3$, $\epsilon^{\infty}_{zz} = 6.5$, $\epsilon^{\infty}_{yy} = 4.6$. The ratio between the number of adjusted parameters (including components of $\hat{\epsilon}^{\infty}$) and the number of experimental points considered was approximately 1/30 for A_u modes and 1/60 for B_u modes. To assess the parameter-adjusting errors caused by the signal noise we have repeated the adjustment of the parameters several times after addition of artificial noise having the dispersion of the real noise to the signal. During this procedure, the values of all of the frequencies ω_{0j} varied by no more than $\pm 1\%$. The plasma frequencies ω_{pj} and damping constants γ_j were less stable: they varied by up to $\pm 15\%$. The angles θ_j of the B_u modes turn out to be quite well defined: they varied on average by $\pm 1^{\circ}$; maximum variation for the 175 cm^{-1} mode was $\pm 5^{\circ}$. This fact confirms the applicability of the current method for determination of polarizations of B_u phonons. It is noteworthy that we succeeded in firmly resolving two closely located B_u modes, at 175 and 179 cm^{-1}. This was possible because, owing to the different polarization angles θ_j, these modes contribute to the three spectra in figure 2 in different ways. The ordinary dispersion analysis technique [12] does not allow one to resolve such overlapping bands. The credibility of the results (especially for the B_u modes) is also seen from the fact that formal fitting of measured spectra with the Fourier series with noise filtering [19] with the same accuracy requires approximately five times as many parameters as we used.

We have established that the previously observed intensive low-lying mode at 37 cm^{-1} belongs to the set of A_u modes (in accordance with the suggestion in [9]). Thus, the behaviour of the reflectivity in figures 2(b) and 2(c) near the low-frequency boundary of the spectral region studied points to the existence of a very low-lying B_u mode in the vicinity of 30 cm^{-1}. Unfortunately, we could not see the left-hand side of this band, so its parameters remain unknown. In this respect it is interesting to note that the analysis of the polarized Raman spectra of single-crystal α-Bi_2O_3 [20] showed, with confidence, that there are no Raman bands lower 50 cm^{-1} (down to 15 cm^{-1}).

The highest frequencies that we observed were 544 cm^{-1} for A_u modes and only 504 cm^{-1} for B_u modes, whereas in [9] frequencies of 598 cm^{-1} and 587 cm^{-1} were reported. The highest frequencies, obtained from polycrystalline reflectance spectra [7], are in accordance with our data.

Inasmuch as the previous measurements of α-Bi_2O_3 IR spectra [6, 7, 9] were made on powder samples, it was impossible to make an assignment of the peculiarities found in the spectra to the A_u and B_u modes. The only attempt at an assignment undertaken in [9] was based on the results of calculations of lattice vibrations performed by the Wilson Green function matrix method. On the whole, the satisfactory correspondence between the frequencies obtained from our analysis and the frequencies reported by other authors [7, 9] is obtained only for modes with wavenumbers lower than 200 cm^{-1}; for the remaining spectral region the correspondence is poorer. Our results agree better with data obtained from the reflectance spectrum [7] than with those from the absorbance spectrum [9]. So the interatomic interactions involving the oxygen atoms determined in [9] need refinements.

The method proposed in the current paper gives more reliable information on phonon frequencies, the problem of mode assignment being solved automatically. New information about polarizations of B_u modes is an additional reference for checking of interatomic potential models. Plasma frequencies should also be used along with other parameters because they contain information about effective ionic charges. Exact information about Bi–O bonding is necessary to provide answers to many questions. In particular, it is of interest for the explanation of recently observed unusual magnetic properties of α-Bi_2O_3 [23]. Besides this, bismuth's complicated valence properties in oxide systems have been

extensively discussed [21, 22].

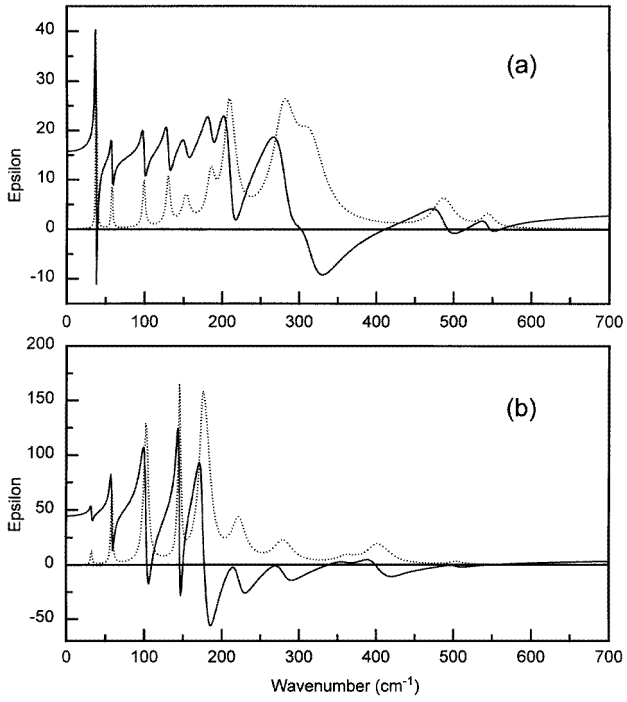

Figure 4. The frequency dependence of the real (solid line) and imaginary (dotted line) parts of ϵ_{yy} (a) and $(1/2)(\epsilon_{xx} + \epsilon_{zz})$ (b).

In figures 4(a) and 4(b) the complex dielectric functions along the ***b***-axis, ϵ_{yy}, and in the *ac*-plane, $(1/2)(\epsilon_{xx} + \epsilon_{zz})$, are shown. The latter combination was chosen in such a form because: (i) it is invariant relative to the rotation of the system of coordinates within the *ac*-plane; (ii) it does not depend on the angles θ_j; (iii) for a cubic crystal it would be equal just to the dielectric function. The maxima of Im $\epsilon(\omega)$ determine the frequencies of the TO modes. From a comparison of figures 4(a) and 4(b) (note the different vertical scales!) we come to an important conclusion that on average B_u modes are significantly more intensive (have greater effective charges) than A_u modes. Correspondingly, plasma frequencies and especially mode strengths of B_u modes are on average greater than those of A_u modes (see table 1). Two B_u modes, at 102 cm^{-1} and 179 cm^{-1}, are the most outstanding as regards strength. Another qualitative difference between the two mode species lies in the frequency distribution of the line intensities: that is, the most intensive A_u modes (excluding the mode at 37 cm^{-1}) are located between 185 cm^{-1} and 314 cm^{-1}, whereas the strongest B_u modes lie in the range from 58 cm^{-1} to 222 cm^{-1}. The observed effective charge distribution anisotropy needs to be explained by calculations in the framework of an interatomic potential model.

It follows from the preliminary results of our calculations as well as from [9] that the lowest IR-active modes with wavenumbers below 150 cm^{-1} are related mainly to displacements of Bi atoms. Optical modes with intermediate wavenumbers are evidently determined by movements of both Bi and O atoms; the highest modes are predominantly connected with oxygen displacements. So we may infer that the intensity of A_u modes

is specified mainly by the effective charges of O atoms, while the intensity of B_u modes pertains equally to Bi and O effective charges.

Using the parameter values obtained, we have derived from equations (3)–(6) approximate values of the components of the static dielectric tensor at room temperature: $\epsilon_{yy}(0) = 15.7$, $\epsilon_{xx}(0) = 37.0$, $\epsilon_{xz}(0) = -0.4$, $\epsilon_{zz}(0) = 60.1$. One can see that the largest value of the static dielectric constant is along the z-axis (perpendicular to the $\boldsymbol{a}$-axis), and the smallest value is along the $\boldsymbol{b}$-axis. Substantial differences between $\epsilon(0)$ in the ac-plane and $\epsilon(0)$ along the $\boldsymbol{b}$-axis are a consequence of the above-mentioned distinction between intensities of A_u and B_u modes. The anisotropy of $\hat{\epsilon}(0)$ within the ac-plane is largely determined by the polarization directions of the B_u modes at 102 cm^{-1} and 179 cm^{-1}, having the largest strengths (table 1).

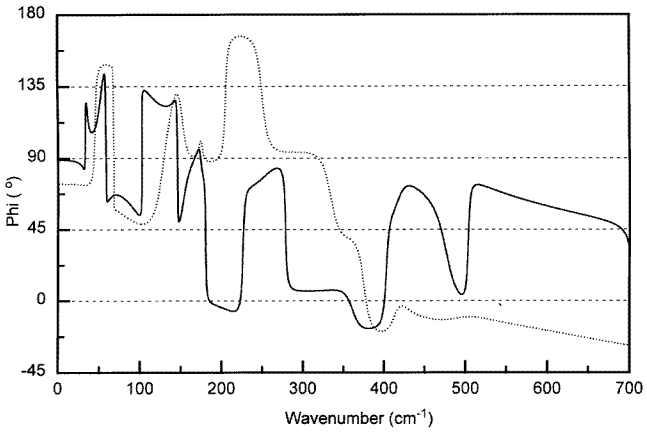

Figure 5. The frequency dependence of the angles φ_R (solid curve) and φ_I (dotted curve) defined by equation (17). Solutions of (17) in different spectral intervals were chosen in such a way as to obtain a continuous resulting function.

One of the key optical features of monoclinic crystals is rotation of the principal dielectric axes within the ac-plane with frequency variation. As long as all of the components of the dielectric tensor are known in the framework of the current model, it is possible to study this effect numerically. The rotation of the dielectric ellipse can be described by the angle between its principal axis, corresponding to the maximal eigenvalue, and the $\boldsymbol{a}$-axis. We must keep in mind, however, that so far we have operated with the complex dielectric tensor as a whole, without separating it into real and imaginary components. $\mathrm{Re}\,\hat{\epsilon}$ and $\mathrm{Im}\,\hat{\epsilon}$ cannot be in general diagonalized in one system of real coordinates [15], but the complex tensor can be diagonalized in the basis of complex vectors $\boldsymbol{e}_u$ and $\boldsymbol{e}_v$ (see section 4), whose x- and z-components may be shifted in phase. Therefore, the value of φ defined by the formula (8) is generally complex. To describe the rotations of the axes by true angles, we have separated the real and imaginary parts of $\hat{\epsilon}$ (the latter is proportional to the optical conductivity: $\mathrm{Im}\,\hat{\epsilon} = 4\pi\hat{\sigma}/\omega$), and calculated the corresponding angles φ_R and φ_I using formulas like (8):

$$\tan 2\varphi_R = \frac{2\,\mathrm{Re}\,\epsilon_{xz}}{\mathrm{Re}\,\epsilon_{xx} - \mathrm{Re}\,\epsilon_{zz}} \qquad \tan 2\varphi_I = \frac{2\,\mathrm{Im}\,\epsilon_{xz}}{\mathrm{Im}\,\epsilon_{xx} - \mathrm{Im}\,\epsilon_{zz}}. \tag{17}$$

In other words, φ_R and φ_I are angles between the $\boldsymbol{a}$-axis and the principal axes of $\mathrm{Re}\,\hat{\epsilon}$ and $\mathrm{Im}\,\hat{\epsilon}$, corresponding to the maximal tensor eigenvalue in the ac-plane. The frequency

dependences of these angles are shown in figure 5. Equations (17) define angles accurate to $\pi/2$; therefore the choice of solutions for different spectral ranges was determined by the continuity of the resulting function. From figure 5 we can see that: (i) the effect of axis rotation in the *ac*-plane in α-Bi_2O_3 is substantial; (ii) the principal axes of $\mathrm{Re}\,\hat{\epsilon}$ and $\mathrm{Im}\,\hat{\epsilon}$ are not collinear (with the exception of at several frequency points, where the curves for φ_R and φ_I intersect). Neglect of the principal axis rotation would result in errors in the determination of the phonon characteristics.

6. Conclusion

For the first time infrared reflectance spectra of single-crystal α-Bi_2O_3 have been reported for different directions and polarizations of the incident wave. A method is proposed for classification of vibrational TO modes and determination of their characteristics, including the orientation of the dipole momentum. It is an extension of the conventional dispersion analysis of IR reflectance spectra to the case of a monoclinic lattice with non-fixed principal dielectric axes. According to this method, the characteristics of B_u modes are determined by the simultaneous treatment of three reflectance spectra for different orientations of the electric field within the *ac*-plane on the basis of relations for the reflectivity derived in section 4. Using this procedure we have obtained and classified almost all of the optical phonons in α-Bi_2O_3. Our measurements revealed large anisotropies of dielectric properties of α-Bi_2O_3: B_u modes turned out to be several times more intense than A_u modes. This means that dipole moments arising in the *ac*-plane from displacements of Bi and O atoms are markedly larger than those appearing parallel to the ***b***-axis. The data obtained can be utilized as a reference for α-Bi_2O_3 lattice dynamic modelling and interatomic potential adjustment. The calculated values of the static dielectric tensor component are useful for understanding anisotropic elastic properties of single-crystal α-Bi_2O_3.

Acknowledgment

We are grateful to Dr A N Ivlev for helpful discussions and assistance during the current research

References

[1] Michel C, Hervieu M, Borel M M, Grandin A, Deslandes F, Provost J and Raveau B 1987 *Z. Phys.* B **68** 421
[2] Maeda H, Tanaka Y, Fukutomi M and Asano T 1988 *Japan. J. Appl. Phys.* **27** L209
[3] Sleight A W, Gillson J L and Bierstedt P E 1975 *Solid State Commun.* **17** 27
[4] Mattheiss L F, Gyorgy E M and Johnson D W 1988 *Phys. Rev.* B **37** 3745
[5] Cava R J, Battlogg B, Krajewski J J, Farrow R, Rupp L W, White A E, Short K, Peck W F and Kometani T 1988 *Nature* **332** 814
[6] Betsch R J and White W B 1978 *Spectrochim. Acta* A **34** 505
[7] Popovic Z V, Thomsen C, Cardona M, Lin R, Stanisic G, Kremer R and Konig W 1988 *Solid State Commun.* **66** 965
[8] Crossley A, Graves P R and Myhra S 1991 *Physica* C **176** 106
[9] Narang S N, Patel N D and Kartha V B 1994 *J. Mol. Struct.* **327** 221
[10] Harwig H A 1978 *Z. Anorg. Allg. Chem.* **444** 151
[11] Poulet H and Mathieu J-P 1970 *Spectres de Vibration et Symetrie des Cristaux* (Paris: Gordon and Breach)
[12] Spitzer W G and Kleinmann D A 1961 *Phys. Rev.* **121** 1324
[13] Barker A S Jr 1964 *Phys. Rev.* **136** 1290
[14] Born B and Huang K 1954 *Dynamical Theory of Crystal Lattices* (Oxford: Clarendon)

[15] Born M and Wolf E 1968 *Principles of Optics* (Oxford: Pergamon)
[16] Landau L D and Lifshitz E M 1975 *Electrodynamics of Continuous Media* (Oxford: Pergamon)
[17] Agranovich V M and Ginzburg V L 1984 *Crystal Optics with Spatial Dispersion and Excitons* vol 42 (Berlin: Springer)
[18] Press W H, Teulkolsky S A, Vetterling W T and Flannery B P 1992 *Numerical Recipes in FORTRAN* (Cambridge: Cambridge University Press)
[19] Kosarev E L and Pantos E 1983 *J. Phys. E: Sci. Instrum.* **16** 537
[20] Denisov V N, Ivlev A N, Lipin A S, Mavrin B N, Orlov V G and Tishchenko E A 1996 *Proc. 21st Int. Conf. on Low Temperature Physics; Czech. J. Phys.* at press
[21] Karlow M A, Cooper S L, Kotz A L, Klein M V, Han P D and Payne D A 1993 *Phys. Rev.* B **48** 6499
[22] Lobo R P S M and Gervais F 1995 *Phys. Rev.* B **52** 13 294
[23] Kharkovskii A I, Nizhankovskii V I, Kravchenko E A and Orlov V G 1996 *Z. Naturf.* a **51** at press